encyclopedia

MDPI

Entry

Perovskite-Type Oxides as Exsolution Catalysts in CO_2 Utilization

Thomas Ruh *, Florian Schrenk, Tobias Berger and Christoph Rameshan

Chair of Physical Chemistry, Montanuniversität Leoben, 8700 Leoben, Austria; florian.schrenk@unileoben.ac.at (F.S.); tobias.berger@unileoben.ac.at (T.B.); christoph.rameshan@unileoben.ac.at (C.R.)

* Correspondence: thomas.ruh@unileoben.ac.at; Tel.: +43-3842-402-4800

Definition: Perovskite-type oxides (ABO_3) are a highly versatile class of materials. They are compositionally flexible, as their constituents can be chosen from a wide range of elements across the periodic table with a vast number of possible combinations. This flexibility enables the tuning of the materials' properties by doping the A- and/or B-sites of the base structure, facilitating the application-oriented design of materials. The ability to undergo exsolution under reductive conditions makes perovskite-type oxides particularly well-suited for catalytic applications. Exsolution is a process during which B-site elements migrate to the surface of the material where they form anchored and finely dispersed nanoparticles that are crucially important for obtaining a good catalytic performance, while the perovskite base provides a stable support. Recently, exsolution catalysts have been investigated as possible materials for CO_2 utilization reactions like reverse water–gas shift reactions or methane dry reforming.

Keywords: CO_2 utilization; perovskite catalysts; exsolution; nanoparticles; closed carbon cycle; zero net emissions; high temperature stability; catalyst design; dry reforming; nanoparticle exsolution

Citation: Ruh, T.; Schrenk, F.; Berger, T.; Rameshan, C. Perovskite-Type Oxides as Exsolution Catalysts in CO_2 Utilization. *Encyclopedia* **2023**, *3*, 1461–1473. https://doi.org/10.3390/encyclopedia3040104

Academic Editors: George Z. Kyzas and Raffaele Barretta

Received: 1 October 2023
Revised: 13 November 2023
Accepted: 21 November 2023
Published: 23 November 2023

1. Introduction

An overwhelming majority of published studies on the topic agree that current global warming is a consequence of human-caused (anthropogenic) climate change [1]. The level of the greenhouse gas CO_2 in the atmosphere—which is the main cause of anthropogenic climate change—rose sharply between the beginning of the Industrial Era (approximately 280 ppm) and today (more than 400 ppm), thus straining the carbon budget (i.e., the amount of carbon that can be released in the atmosphere while still limiting global warming to a given temperature difference) [2]. Therefore, efforts are being undertaken to reduce CO_2 to achieve net zero emissions (e.g., the European Green Deal [3] aims for climate neutrality of the European Union by 2050).

Closing the carbon cycle via CO_2 conversion is a possible way towards meeting this goal. This means no longer treating emitted CO_2 as a waste gas but as a readily available carbon source for base materials or fuels. A schematic depiction of such a closed carbon cycle in industries is shown in Figure 1. Flue gas from industries and power generation is captured and converted. The products can be used as feedstock in the chemical industry or as fuels which can be stored for later use. CO_2 conversion can be driven in different ways. In a 2019 review, De Luna et al. discussed the question of how CO_2 electrolysis (i.e., electrochemical processes) could be a pathway to replacing the chemicals and fuels produced petrochemically [4]. In the authors' own work, we investigate a different approach to achieve CO_2 conversion. Instead of electrolysis, seemingly straightforward reactions like the reverse water–gas shift reaction (rWGS, Equation (1)) or the dry reforming of methane (DRM, Equation (2)) are used to directly transform CO_2 into CO or syngas (a mixture of CO and H_2), respectively.

$$CO_{2(g)} + H_{2(g)} \rightleftharpoons CO_{(g)} + H_2O_{(g)} \left(\Delta H_r^{298} = +42 \text{ kJ mol}^{-1}\right) \quad (1)$$

$$CO_{2(g)} + CH_{4(g)} \rightleftharpoons 2\,CO_{(g)} + 2\,H_{2(g)} \left(\Delta H_r^{298} = +247 \text{ kJ mol}^{-1}\right) \quad (2)$$

Figure 1. Closing the carbon cycle: CO_2 from flue gas emitted from industries (1) is captured (2) and converted (3) into fuels (e.g., for aviation, (4)) or feedstocks for the chemical industry. Produced fuels can be stored or used (e.g., for transportation or heating, (5)) the CO_2 set free here is then recycled and used for another conversion. To operate conversion sustainably, renewable energy (6) is used both directly during the conversion and indirectly during the production of green H_2 (7), which is needed, for instance, in rWGS reactions.

Due to its stability, reactions using CO_2 as a raw material necessitate the use of a catalyst for activation. Furthermore, CO_2 activation processes demand large amounts of energy. This opens up energy storage as a second potential application of CO_2 conversion (apart from the reduction of emissions), as electrical energy (ideally renewably generated with solar panels, wind turbines, geothermal plants. . .) is converted into chemical energy of fuels that can be stored more easily.

For both rWGS and DRM, a large number of diverse catalytically active materials have been extensively researched, for instance, supported catalysts based on noble metals [5,6] or Ni [7]. However, there are drawbacks for these catalysts, e.g., Ni-based catalysts are vulnerable to deactivation via carbon deposition [8] and catalysts using noble metals, while not as susceptible to coking [9], are expensive. Additionally, high temperatures are required when performing rWGS or DRM, which can cause nanoparticles to sinter together, thus reducing the catalytically active surface. This means that suitable catalysts for large-scale applications need to be stable at high temperatures, resist coking, and contain catalytically active elements that are available at the surface (e.g., as nanoparticles, which should not be prone to sintering in order to maintain their activity). A promising class of materials for use as such CO_2 conversion catalysts are perovskite-type oxides due to their stability at high temperatures, their compositional flexibility, and their ability to undergo exsolution:

Perovskite-type oxides share the general formula ABO_3, where A and B are two cations of different sizes that are arranged as shown in Figure 2a. The larger A-site cations make up the corners of the unit cell; the smaller B-site cations fill the center of the cell and are

octahedrally coordinated by oxygen atoms. Depending on the differences in the atomic radii of the cations, cubic, orthorhombic, or rhombohedral cells can occur. A- and B-site elements can vary over a wide range of the periodic table, paving the way to a vast number of possible materials. Moreover, both sites can be doped, which not only introduces an even larger number of possible materials, but also facilitates a material design approach, as the materials' properties can be tuned with the specific applications in mind [10]. Aside from catalysis, applications of perovskite-type oxides include, for instance, electrodes used in electrochemistry or fuel cells [11–13].

Exsolution is a striking property of perovskite-type oxides that causes their particular potential as catalysts [14], especially with respect to the requirements of finely dispersed and sinter-resistant nanoparticles. Exsolution is an extensively studied process [15–17], during which the surface of the perovskite is decorated by nanoparticles made up of B-site elements (schematically shown in Figure 2b): Under reducing conditions, B-site cations move to the surface of the material, where they form finely dispersed and well anchored nanoparticles. The make-up (oxidic vs. metallic composition) of these nanoparticles can be tuned by the composition of the perovskite (influenced by doping) [10] as well as the exsolution conditions [17], thus allowing even more control of the specific catalytic properties of the material.

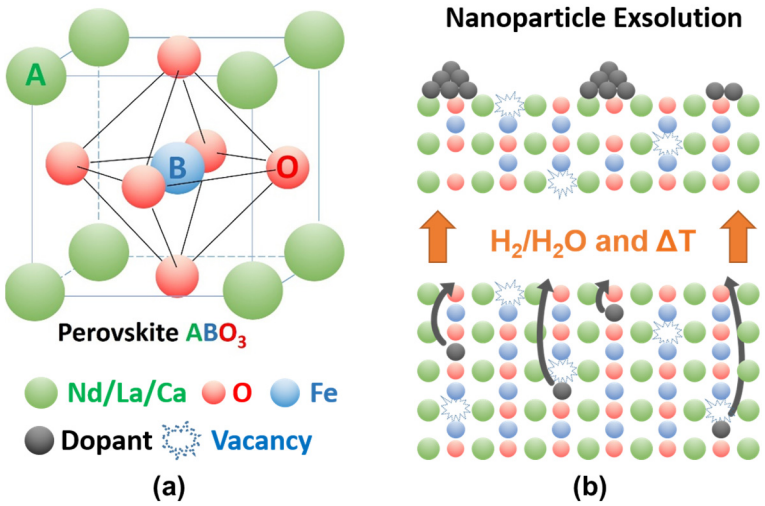

Figure 2. "(**a**) The perovskite structure and (**b**) a schematic depiction of the exsolution process. In a wet hydrogen atmosphere and under heat treatment, additional oxygen vacancies are created, and dopant atoms reduce, resulting in their migration from the bulk to the surface, where they form nanoparticles." Reprinted from [18] under CC-BY 4.0.

This entry aims to showcase how perovskite-type oxides as catalysts in CO2 conversion processes are investigated to assess their suitability.

2. Materials—Synthesis and Characterization

As mentioned before, CO_2 conversion processes impose a set of requirements (high temperature stability, coking resistance, nanoparticle/active site stability. . .) on catalyst materials. A deeper understanding of catalysts in general and detailed insights into the structure–property relations necessary to tune a catalyst as well as the intensive characterization and controlled synthesis of precursor materials, are crucial. A wide array of different methods is used to gain these insights.

2.1. Synthesis of Perovskites

Common methods used to prepare powder samples of perovskite-type oxides are solid-state [19] and sol-gel synthesis (e.g., Pechini synthesis [10]) as well as flame-assisted spray pyrolysis [20,21].

Solid-state and sol-gel methods use precursors (oxides, carbonates, or nitrates are widely used in perovskite synthesis) that are either dispersed in small amounts of volatile solvents like acetone (in case of the solid-state route [19]) or dissolved, for instance, in water or nitric acid (sol-gel [10]). Then, the precursors are mixed in the desired stoichiometric ratio. Additionally, complexing agents such as citric acid are added during sol-gel processes. In both synthesis routes, the liquid is evaporated. During the solid-state method, the remaining slurry is calcined directly at high temperatures and finely ground down (e.g., via ball milling). In sol-gel synthesis, the gel that remains after evaporation is heated until self-ignition, which leads to a sponge-like structure that is milled to a fine powder which, in turn, is calcined as well. Additional grinding and calcination steps might be necessary to achieve phase purity [10,19].

The low surface area of the resulting powders is a major drawback of the above-mentioned methods, which is especially problematic for catalytic materials. The reason for this is sintering, which happens during calcination steps. A workaround to the manufacture of powders with high surface areas is liquid-feed flame-assisted spray pyrolysis. The precursors (usually salts with organic anions like ethyl hexanoate) are dissolved as well, mixed in the proper ratio, and fed via a pressurized nozzle into a CH_4/O_2 flame where nanocrystalline powders are formed, which are collected and used for characterization [21].

Alternative methods of synthesizing perovskite oxides include, but are not limited to, the co-precipitation method, hydrothermal synthesis, and microwave synthesis. These methods are only briefly described here; however, there is already extensive literature discussing this topic [22]. During co-precipitation, all cations are mixed and precipitated simultaneously either due to the addition of a reagent or thermal decomposition [23]. However, precise control of the procedure is a necessity to obtain a phase-pure product. In hydrothermal synthesis, the reaction is performed in an aqueous solution but at elevated temperatures and pressures [24]. As an alternative heating source, microwaves can be used to very quickly heat an aqueous solution of dissolved precursors.

2.2. X-ray Diffraction

Ex situ X-ray Diffraction (XRD) under ambient conditions can be used to check the phase purity after synthesis or additional calcination steps, as the presence of impurities causes additional reflexes to appear [18].

Moreover, the emergence of nanoparticles after exsolution experiments (in the form of additional oxidic or metallic phases) as well as the continued stability of the perovskite lattice after (high temperature) catalytic tests (see Section 3.1) can be verified [15]. Additionally, some common deactivation products (e.g., carbonates, graphite) can be observed via XRD.

XRD measurements can also be performed in situ or operando to track structural changes during reactions (see Section 3.2).

2.3. Micrsocopic Characterization—SEM and TEM

Scanning Electron Microscopy (SEM) and Transmission Electron Microscopy (TEM) are methods that are routinely used to characterize the surfaces of catalyst materials as well as nanoparticles after exsolution [25].

SEM images provide information not only about the presence of nanoparticles (i.e., whether or not exsolution occurred, for example, see the left side of Figure 3 [18]) and their sizes, shapes, and population density, coupled with Energy Dispersive X-ray Spectroscopy (EDX) [26], it can also give elemental information. The image shown on the right-hand side of Figure 3 [18], for instance, reveals iron accumulation in the locations of the nanoparticles, lending credibility to the conclusion that exsolution of iron particles has occurred.

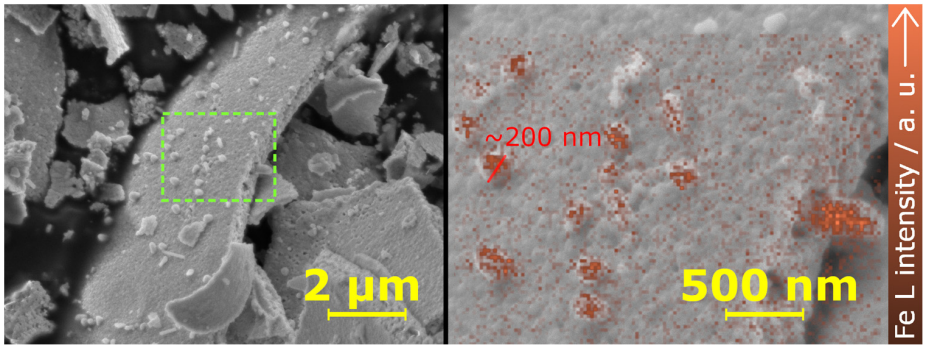

Figure 3. "SEM images of the [$Nd_{0.9}Ca_{0.1}FeO_{3-\delta}$] sample after reduction in wet H_2 at 650 °C. The image on the right is a detail (green box) of the image on the left at a higher magnification. Exsolved nanoparticles are visible at the perovskite surface, with diameters of around 200 nm. An EDX mapping was performed of the magnified area. The Fe distribution, characterized by the net intensity of the Fe *L* peak, is shown as an overlay. The particles visible in the secondary electron image coincided with a higher Fe concentration." Reprinted from [18] under CC-BY 4.0.

Information about the anchorage as well as geometric data (orientation of the exposed face, distances between lattice planes. . .) of the nanoparticles can be extracted from TEM images. The latter requires a high resolution though. The elemental make-up of the particles can be studied from TEM+EDX as well [25]. Additionally, environmental TEM can be used to visualize the exsolution process on an atomic scale [27]. In this study, Neagu et al. observed the formation of Ni metal nanoparticles from $La_{0.43}Ca_{0.37}Ti_{0.94}Ni_{0.06}O_3$ in situ using environmental TEM, as seen in Figure 4. They confirmed that the particles grow while maintaining their initial nucleation positions. During the growth, the perovskite lattice rises around the particle, leading to anchoring of the particles into the lattice [27].

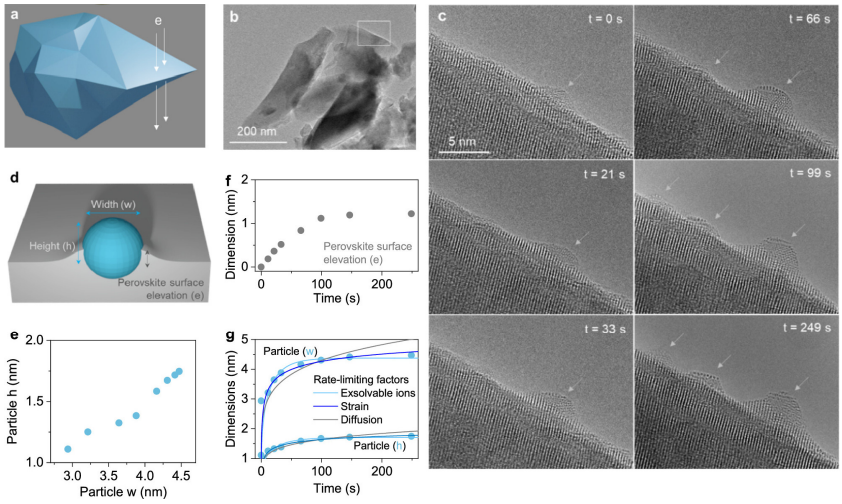

Figure 4. "Particle–socket formation during in situ growth under H_2. (**a**) Schematic illustration of a perovskite particle in a suitable orientation for monitoring one of its edges by electron microscopy imaging. (**b**) TEM of a $La_{0.43}Ca_{0.37}Ni_{0.06}Ti_{0.94}O_3$ perovskite powder, highlighting an edge of a grain where particle growth was followed. (**c**) Selected region followed throughout the reduction process at 900 °C, under H_2, showing snapshots at different times (*t*) of the gradual formation of a particle–socket and nucleation of two additional particles. (**d**) Schematic illustration of a particle within a socket annotated with the dimensions used to quantify its evolution over time. (**e**) Plot of the particle height vs. width. (**f**) Plot of the elevation of the perovskite lattice in the region adjacent to the particle, as a function of time. (**g**) Plot of the particle width and height as a function of time together with various models identifying the rate-limiting step in particle growth." Reprinted with permission from [27]. Copyright 2019 American Chemical Society.

In a study by Kim and co-workers [28], the reduction time and temperature of $La_{0.6}Ca_{0.2}Ni_{0.25}Ti_{0.75}O_3$ were varied. It was found that at reduction temperatures of 800 °C and below (in this case 600 °C, 700 °C, and 800 °C), only a small difference in the size of the formed nanoparticles occurred when increasing the reduction time from 3 h to 24 h. All exsolved particles were spherical at these temperatures, and the size increased with an increasing temperature. Going to an even higher temperature of 900 °C showed the expected trend when reducing for 3 h. However, when the reduction time was increased to 24 h, faceting of the nanoparticles occurred, forming triangular and pyramidal shapes with larger sizes. At 1000 °C, the faceted nanoparticles had already formed after 3 h of reduction but doubled in size after 24 h. A comparison of the catalytic activity between the spherical and faceted nanoparticles for DRM revealed that the faceted nanoparticles were not only more active but also exhibited greater stability. This was also found in the comparison of smaller particles exsolved in situ versus bigger particles exsolved during a reductive pre-treatment in the authors' own work [29]. Interestingly for systems where Ni nanoparticles were deposited on SiO_2, an inverse trend (bigger nanoparticles lead to decreased catalytic activity) was found [30].

In a study by Gao et al. [31], analyzing the energetics of exsolution, four distinct steps in the process were proposed: diffusion, reduction, nucleation, and particle growth. As grain boundaries are preferential pathways for diffusion, it becomes clear why they are also preferred nucleation sites for nanoparticles.

2.4. X-ray Photoelectron Spectroscopy

X-ray Photoelectron Spectroscopy (XPS) is a surface sensitive method that can be used to characterize surface species in more detail, for instance, the nature of exsolved nanoparticles (oxidic vs. metallic) or the oxidation states of surface atoms before and after a reaction [32].

In situ XPS measurements are particularly useful to elucidate the reaction mechanisms even further by observing changes to surface species under the reaction conditions and to monitor the formation of suspected additional surface species, like carbonaceous deposits on the surface (see Section 3.3).

2.5. Theoretical Modeling

Electronic structure calculations are another powerful tool to further understand the properties of the materials under investigation as well as to predict novel candidates for given applications.

Density Functional Theory (DFT) can be utilized to study the effects of doping on the electronic properties (for instance, changes in conductivity caused by A-site doping [33]) or on the atomic structure (changes in lattice parameters, atomic distances, and angles), which are of particular interest, as exsolution requires atoms to diffuse through the bulk to the surface [18]. Thermodynamic quantities, like enthalpies of formation [34], energy barriers during diffusion [35], defect formation energies [36], or energetics of adsorption processes (especially relevant for heterogeneously catalyzed gas phase reactions) [37], can be calculated as well. Moreover, DFT studies are a useful tool for the proposal of possible mechanisms and/or reaction pathways, for instance, Huang et al. investigated the effect of exsolved Ni nanoparticles on La-based perovskite surfaces on water–gas shift reactions [38].

As mentioned before, perovskite-type oxides span a vast compositional space due to the large number of viable compositions with possible doping on top. High-throughput DFT calculations are needed to screen this space. In a recent effort to create a dataset of multinary perovskite-type oxides, Bare et al. [39] generated almost 70,000 perovskite-type oxides and optimized their structures to assess their stability (by predicting the formation and decomposition energies). The resulting test set can be used for data mining or the training of machine learning models to find potential new catalyst materials without having to synthesize and manually test a huge number of candidates.

3. Catalytic Tests and In Situ/Operando Measurements

So far, the characterization methods presented only address ex situ measurements (meaning the measurement conditions do not represent exsolution or reaction conditions). While they still give valuable information by allowing comparisons between the initial pristine state of a catalyst before any further treatment and the states after exsolution has been triggered or reactions have been performed, the analysis of the materials during reactions or exsolution and at higher temperatures or pressures is crucial to obtain a more detailed picture of the catalyst's properties. To achieve this, in situ or operando measurements have to be performed, for instance, to assess the catalytic performance (by tracking the conversion of CO_2 or the yield of the respective product), to monitor the stability of the perovskite lattice, to track structural changes due to exsolution (including the emergence of newly exsolved nanoparticles), or to observe the possible formation of additional phases (e.g., carbonaceous species) that might affect the catalytic activity [40].

3.1. Catalytic Tests

Catalytic tests are the method of choice for assessing the suitability and performance of any material as a catalyst for a reaction. Not only the catalytic activity itself is of interest, the suppression of side reactions (either via modifying the material itself [41] or by choosing proper reaction conditions [29]) to increase the selectivity, the long-term stability of the material (in terms of a reproducible and continued performance) to ensure the viability as an industry catalyst with extended usability [42], or, more specific to exsolution catalysts, the reversibility of nanoparticle formation which enables the regeneration of the catalytically active surface [43], are examples of factors that have to be investigated intensively to understand materials well enough to design a catalyst.

In Figure 5 and Table 1, the specific activities with respect to the rWGS of various newly synthesized mixed iron-based perovskites are compared (with the well-known $La_{1-x}Sr_xFeO_{3-\delta}$ (LSF) as a reference) at different temperatures [44]. Multiple effects of the elemental composition and doping are visible. Switching the main A-site constituent from La to Nd increases the specific activity, while the effect of the doping concentration on the A-site follows no clear-cut trend; in case of lanthanum, increasing the Ca content appears to be advantageous, while the reverse is true for neodymium. Moreover, introducing B-site doping raises the activity even further with both Ni and Co beneficially affecting the catalyst's performance (Ni more so than Co).

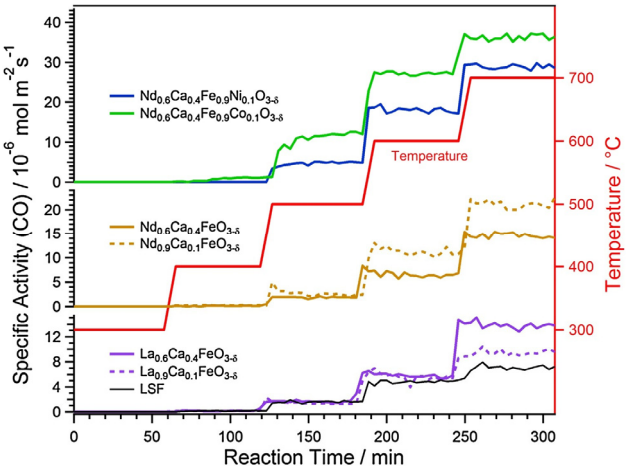

Figure 5. "Comparison of rWGS results. The reaction rates of CO formation are displayed as surface specific activities in mol m^{-2} s^{-1} (note the different scales). LSF is included as benchmark (black line). For the reactions a 1:1 gas mixture of H_2 and CO_2 was used, and the temperature was increased in steps of 100 °C from 300 °C to 700 °C. For all temperatures, Co- and Ni-doped samples exhibited the best activities." Reprinted from [44] under CC-BY 4.0.

Table 1. "BET surface areas, average specific activities calculated for CO production during rWGS at 600 °C and WHSVs of the respective measurements for all investigated perovskite materials" [44]. Accompanying table to Figure 5. Reprinted from [44] under CC-BY 4.0.

Catalyst	Surface Area $m^2\ g^{-1}$	Specific Activity $10^{-6}\ mol\ m^{-2}\ s^{-1}$	WHSV $L\ g^{-1}\ h^{-1}$
$La_{0.9}Ca_{0.1}FeO_{3-\delta}$	3.8	5.7	24.6
$La_{0.6}Ca_{0.4}FeO_{3-\delta}$	2.8	5.9	34.1
$Nd_{0.9}Ca_{0.1}FeO_{3-\delta}$	2.2	11.3	32.7
$Nd_{0.6}Ca_{0.4}FeO_{3-\delta}$	1.5	6.6	20.5
$Nd_{0.6}Ca_{0.4}Fe_{0.9}Ni_{0.1}O_{3-\delta}$	1.6	18.0	36.0
$Nd_{0.6}Ca_{0.4}Fe_{0.9}Co_{0.1}O_{3-\delta}$	1.2	27.2	32.1
commercial LSF	5.7	4.8	28.8

3.2. In Situ XRD

The structural properties of catalysts play important roles for both the actual catalytic activity of the material as well as the stability. Therefore, it is necessary to investigate candidate materials with respect to their stability under realistic conditions (e.g., high temperatures during reactions [45] or under reaction atmospheres). Furthermore, changes in the material (both in bulk, for instance (partial) decomposition, or at the surface, like exsolution or the formation of impurity phases [29,44,46]) caused by reaction conditions need to be studied as well, especially if catalyst design is the goal. In situ XRD allows us to address these questions.

Figure 6 shows a series of in situ XRD measurements performed on a mixed perovskite with Ca-doping on the A- and Co-doping at the B-site at elevated temperatures in a reducing atmosphere (humid H_2) [18]. Over the whole temperature range, the perovskite lattice is stable (perovskite reflexes marked with P are present at all temperatures and hardly exhibit any changes in intensity). Additional peaks start to appear from 575 °C with the onset of nanoparticle exsolution. A Fe/Co bcc phase emerges, which becomes more pronounced with an increasing temperature. Moreover, unwanted CaO begins to appear at around 37° above 600 °C, probably due to A-site Ca^{2+} migrating to the surface where CaO is formed, and, in turn, catalytic activity is reduced due to a loss in the active surface. In recent literature, it was shown that exsolved nanoparticles exhibit outstanding stability under reducing conditions. Zang et al. [47] performed stability tests over 200 h and observed that the nanoparticle size did not change significantly after an initial forming phase.

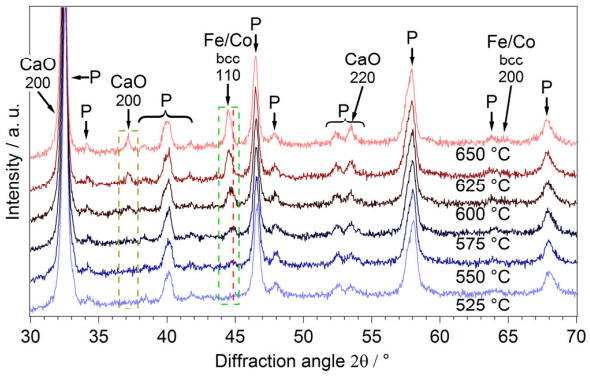

Figure 6. "Diffractograms of the [$Nd_{0.6}Ca_{0.4}Fe_{0.9}Co_{0.1}O_{3-\delta}$] sample during the reduction with humid H_2 at increasing temperature. A new phase, which could be assigned to bcc Fe/Co, was formed above 550 °C—the corresponding (110) reflection is marked by the green box. A shift of the corresponding peak to lower angles was observed at higher temperatures, which was stronger than expected from thermal expansion (compare position to red line). At 600 °C, a CaO phase (brown box) appeared. Both the metallic bcc phase and the CaO phase were more prominent at higher temperatures, while the perovskite structure (reflections labelled 'P'; for the respective hkl indices, cf. Figure 2) stayed intact." Reprinted from [18] under CC-BY 4.0.

3.3. In Situ XPS

As mentioned before, XPS is a method that allows us to study the surface of a given material closely. Changes in the oxidation states of the constituent atoms of the materials accompany the formation of metallic nanoparticles during exsolution. XPS is particularly well-suited to the monitoring of these changes at a quantitative level. Additionally, surface impurities (carbon species) or deposits of inactive solid phases (e.g., oxides of A-site constituents already mentioned in the previous section) can be observed as well.

Figure 7 illustrates how XPS spectra can be used to follow changes to a perovskite surface (and possibly present nanoparticles) under reducing conditions [17]: After an initial oxidizing step in oxygen, only oxidic iron—blue and green contributions to the main peak—is observed (top spectrum), which corresponds to bulk iron cations. By switching to a reducing atmosphere (wet hydrogen), notable exsolution can occur by the shoulder that begins to develop on the right-hand side of the iron peak, which is caused by the emergence of metallic iron (red contribution to the fit). Going to higher temperatures gradually increases the amount of metallic iron (second and third spectra from the top). Adding a negative bias leads to more strongly reducing conditions which, in turn, causes even more metallic iron to appear.

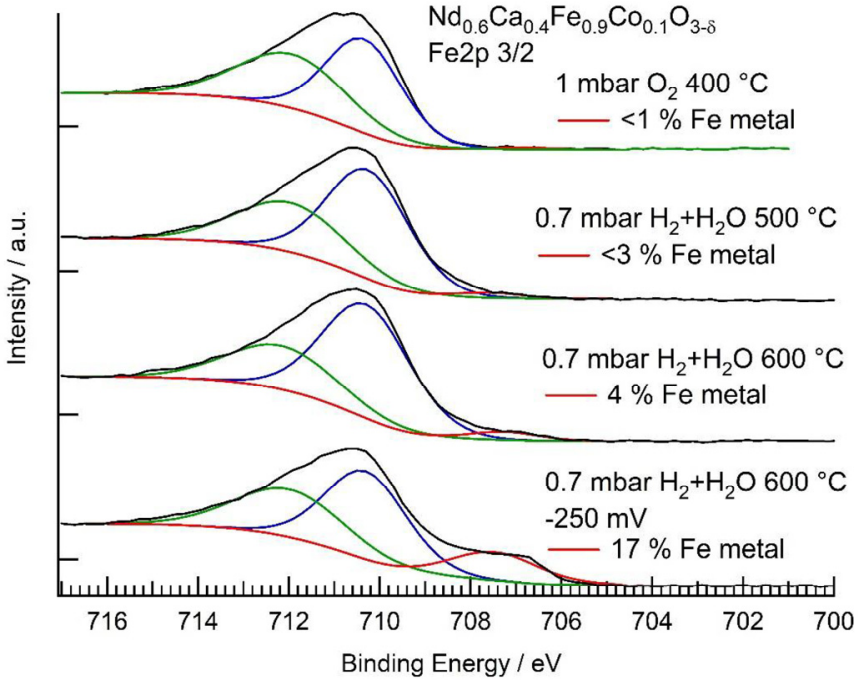

Figure 7. "Fe2p 3/2 signals for each experiment step. The contributions are assigned to Fe^0 (red) and a combination of two components for the asymmetric oxide peak (blue and green). The sample was first heated in O_2 to 400 °C. Then, the gas phase was switched to H_2 + H_2O at 500 °C. In a next step, the temperature was increased to 600 °C. Finally, a bias voltage of −250 mV was applied. A stepwise increase of the contribution of metallic Fe is clearly visible with increasing strength of reduction." Reprinted from [17] under CC-BY 4.0.

The deposition of (often) unwanted species on the surface (e.g., carbonaceous species during catalytic reactions—a process called coking that leads to deactivation of the catalyst) can be followed by XPS as well. Figure 8 shows the temperature-dependent formation of carbon species on an iron-based perovskite used as a DRM catalyst [29]. At moderate temperatures, small amounts of carbon on the surface could be observed, which disappeared at higher temperatures, thus highlighting the coking resistance of perovskite-type oxides.

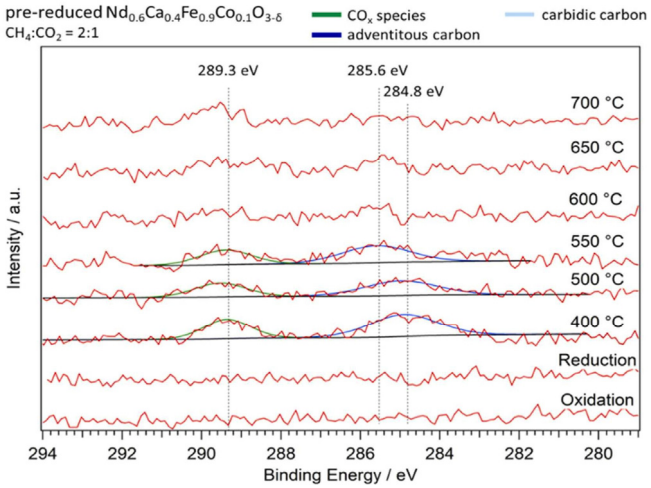

Figure 8. "Comparison of the C1s spectra of the reduced [$Nd_{0.6}Ca_{0.4}Fe_{0.9}Co_{0.1}O_{3-\delta}$] in DRM conditions [. . .]. No catalyst exhibits excessive coking and complete coverage of the surface. The carbon species found could be identified as carbonate species, adventitious carbon, graphitic carbon, and gas phase species. (. . .)" Only sample b of the original figure from reference [29] is shown here to illustrate information gained by XPS. Reprinted in part from [29] under CC-BY 4.0.

4. Conclusions

Perovskite-type oxides are very promising materials for catalysis in general, due to their vast compositional flexibility (which is further enlarged by the possibility of doping on both cationic lattice sites) and their exsolution capabilities. The perovskite lattice forms the oxidic backbone (which, in many cases, is stable up to very high temperatures), while certain constituent atoms migrate to the surface to form nanoparticles under reducing conditions. Choosing the proper elemental make-up of the perovskite (for instance, via the doping of highly catalytically active elements) leads to a perovskite surface that is decorated with nanoparticles that can serve as active sites during catalytic reactions. For the design of an optimal catalyst, several aspects must be considered:

(1) The stability of the material: To achieve the synthesis of a phase-pure catalyst, the thermodynamic requirements for forming a stable phase have to be fulfilled. Databases like the one from Bare et al. [39] can be used as guidelines.

(2) A-site composition: Even though materials on the A-site have not been as deeply studied as materials on the B-site, several design principles are common. Lanthanoids such as La, Nd, Pr, or Sm are often used as major components on the A-site. Their ionic radii make them ideally suited elements to use together with transition metals on the B-site. Additionally, divalent ions such as Ca, Sr, or Ba are often doped on the A-site. This promotes the formation of oxygen vacancies and/or the oxidation of other elements in the material, thus enabling exsolution.

(3) B-site composition: The B-site is often made up of one or more transition metals. The main concern in choosing the B-site is the nature of the nanoparticles that one wants to exsolve. Often, the B-site is made from a base element such as Fe or Ti, which is then doped with the desired exsolving element (e.g., Cu, Co, Ni, . . .). One has to keep in mind that the element to be exsolved should be more easily reducible than the base element.

Currently, these materials are being investigated with respect to their suitability in CO_2 utilization reactions like reverse water–gas shift or the dry reforming of methane, with very encouraging results already published in literature.

A deeper understanding of perovskite oxides can be obtained by a variety of methods like (in situ/operando) X-ray Diffraction, (in situ) X-ray Photoelectron Spectroscopy, and Scanning and Transmission Electron Microscopy. Moreover, their behaviors under reaction conditions (stability, side reactions. . .) need to be well understood in order to design cata-

lysts that make use of the beneficial properties that many perovskites share (such as stability at high temperatures, resilience against coking, sinter-resistant exsolved nanoparticles).

Author Contributions: Conceptualization, T.R. and C.R.; formal analysis, T.B., F.S. and T.R..; resources, C.R.; data curation, T.B. and F.S.; writing—original draft preparation, T.R.; writing—review and editing, T.R., F.S., T.B. and C.R.; visualization, F.S.; supervision, C.R.; project administration, C.R.; funding acquisition, C.R. All authors have read and agreed to the published version of the manuscript.

Funding: The research presented here was funded by the European Research Council (ERC) under the European Union's Horizon 2020 research and innovation programme, grant agreement no. 755744/ERC—Starting Grant TUCAS, by the Austrian Science Fund (FWF) through project SFB-F81 "Taming Complexity in materials modeling" (TACO), and by the Agency for Education and Internationalisation (OeAD) on behalf of the Austrian Ministry of Education, Science and Research under the Sparkling Science 2.0 program (project SPSC_01_015–CO2 Umwandlung).

Data Availability Statement: The data presented in this study are available on request from the corresponding author.

Acknowledgments: We would like to thank the "HTL Bau und Design Innsbruck" for providing Figure 1.

Conflicts of Interest: The authors declare no conflict of interest.

References

1. Lynas, M.; Houlton, B.Z.; Perry, S. Greater than 99% consensus on human caused climate change in the peer-reviewed scientific literature. *Env. Res. Lett.* **2021**, *16*, 114005. [CrossRef]
2. Friedlingstein, P.; O'Sullivan, M.; Jones, M.W.; Andrew, R.M.; Gregor, L.; Hauck, J.; Le Quere, C.; Luijkx, I.T.; Olsen, A.; Peters, G.P.; et al. Global Carbon Budget 2022. *Earth Syst. Sci. Data* **2022**, *14*, 4811–4900. [CrossRef]
3. Communication from the Commission to the European Parliament. The European Green Deal. Available online: https://eur-lex.europa.eu/legal-content/EN/TXT/?uri=COM%3A2019%3A640%3AFIN (accessed on 28 September 2023).
4. De Luna, P.; Hahn, C.; Higgins, D.; Jaffer, S.A.; Jaramillo, T.F.; Sargent, E.H. What would it take for renewably powered electrosynthesis to displace petrochemical processes? *Science* **2019**, *364*, eaav3506. [CrossRef] [PubMed]
5. Matsubu, J.C.; Yang, V.N.; Christopher, P. Isolated Metal Active Site Concentration and Stability Control Catalytic CO_2 Reduction Selectivity. *J. Am. Chem. Soc.* **2015**, *137*, 3076–3084. [CrossRef]
6. Pakhare, D.; Spivey, J. A review of dry (CO_2) reforming of methane over noble metal catalysts. *Chem. Soc. Rev.* **2014**, *43*, 7813–7837. [CrossRef]
7. Daza, C.E.; Gallego, J.; Moreno, J.A.; Mondragon, F.; Moreno, S.; Molina, R. CO_2 reforming of methane over Ni/Mg/Al/Ce mixed oxides. *Catal. Today* **2008**, *133*, 357–366. [CrossRef]
8. Usman, M.; Daud, W.; Abbas, H.F. Dry reforming of methane: Influence of process parameters-A review. *Renew. Sustain. Energy Rev.* **2015**, *45*, 710–744. [CrossRef]
9. Hou, Z.; Chen, P.; Fang, H.; Zheng, X.; Yashima, T. Production of synthesis gas via methane reforming with CO_2 on noble metals and small amount of noble-(Rh-) promoted Ni catalysts. *Int. J. Hydrogen Energy* **2006**, *31*, 555–561. [CrossRef]
10. Lindenthal, L.; Rameshan, R.; Summerer, H.; Ruh, T.; Popovic, J.; Nenning, A.; Löffler, S.; Opitz, A.K.; Blaha, P.; Rameshan, C. Modifying the Surface Structure of Perovskite-Based Catalysts by Nanoparticle Exsolution. *Catalysts* **2020**, *10*, 268. [CrossRef]
11. Hwang, J.; Rao, R.R.; Giordano, L.; Katayama, Y.; Yu, Y.; Shao-Horn, Y. Perovskites in catalysis and electrocatalysis. *Science* **2017**, *358*, 751–756. [CrossRef]
12. Nishihata, Y.; Mizuki, J.; Akao, T.; Tanaka, H.; Uenishi, M.; Kimura, M.; Okamoto, T.; Hamada, N. Self-regeneration of a Pd-perovskite catalyst for automotive emissions control. *Nature* **2002**, *418*, 164–167. [CrossRef]
13. Kwon, O.; Sengodan, S.; Kim, K.; Kim, G.; Jeong, H.Y.; Shin, J.; Ju, Y.W.; Han, J.W. Exsolution trends and co-segregation aspects of self-grown catalyst nanoparticles in perovskites. *Nat. Commun.* **2017**, *8*, 15967. [CrossRef] [PubMed]
14. Neagu, D.; Tsekouras, G.; Miller, D.N.; Menard, H.; Irvine, J.T.S. In situ growth of nanoparticles through control of non-stoichiometry. *Nat. Chem.* **2013**, *5*, 916–923. [CrossRef]
15. Neagu, D.; Oh, T.S.; Miller, D.N.; Menard, H.; Bukhari, S.M.; Gamble, S.R.; Gorte, R.J.; Vohs, J.M.; Irvine, J.T.S. Nano-socketed nickel particles with enhanced coking resistance grown in situ by redox exsolution. *Nat. Commun.* **2015**, *6*, 8120. [CrossRef] [PubMed]
16. Lindenthal, L.; Huber, J.; Drexler, H.; Ruh, T.; Rameshan, R.; Schrenk, F.; Loeffler, S.; Rameshan, C. In Situ Growth of Exsolved Nanoparticles under Varying rWGS Reaction Conditions-A Catalysis and Near Ambient Pressure-XPS Study. *Catalysts* **2021**, *11*, 1484. [CrossRef]
17. Rameshan, R.; Nenning, A.; Raschhofer, J.; Lindenthal, L.; Ruh, T.; Summerer, H.; Opitz, A.K.; Huber, T.M.; Rameshan, C. Novel Sample-Stage for Combined Near Ambient Pressure X-ray Photoelectron Spectroscopy, Catalytic Characterization and Electrochemical Impedance Spectroscopy. *Crystals* **2020**, *10*, 947. [CrossRef]

18. Lindenthal, L.; Ruh, T.; Rameshan, R.; Summerer, H.; Nenning, A.; Herzig, C.; Loffler, S.; Limbeck, A.; Opitz, A.K.; Blaha, P.; et al. Ca-doped rare earth perovskite materials for tailored exsolution of metal nanoparticles. *Acta Crystallogr. B* **2020**, *76*, 1055–1070. [CrossRef]
19. Neagu, D.; Irvine, J.T.S. Enhancing Electronic Conductivity in Strontium Titanates through Correlated A and B-Site Doping. *Chem. Mater.* **2011**, *23*, 1607–1617. [CrossRef]
20. Simmance, K.; Thompsett, D.; Wang, W.L.; Thiebaut, B. Evaluation of perovskite catalysts prepared by flame spray pyrolysis for three-way catalyst activity under simulated gasoline exhaust feeds. *Catal. Today* **2019**, *320*, 40–50. [CrossRef]
21. Koirala, R.; Pratsinis, S.E.; Baiker, A. Synthesis of catalytic materials in flames: Opportunities and challenges. *Chem. Soc. Rev.* **2016**, *45*, 3053–3068. [CrossRef]
22. Assirey, E.A.R. Perovskite synthesis, properties and their related biochemical and industrial application. *Saudi Pharm. J.* **2019**, *27*, 817–829. [CrossRef] [PubMed]
23. Pérez-Coll, D.; Núñez, P.; Frade, J.R.; Abrantes, J.C.C. Conductivity of CGO and CSO ceramics obtained from freeze-dried precursors. *Electrochim. Acta* **2003**, *48*, 1551–1557. [CrossRef]
24. Shandilya, R.; Rai, R.; Singh, J. Review: Hydrothermal technology for smart materials. *Adv. Appl. Ceram.* **2015**, *115*, 354–376. [CrossRef]
25. Ruh, T.; Berkovec, D.; Schrenk, F.; Rameshan, C. Exsolution on perovskite oxides: Morphology and anchorage of nanoparticles. *Chem. Comm.* **2023**, *59*, 3948–3956. [CrossRef] [PubMed]
26. Goodhew, P.J.; Humphreys, J. *Electron Microscopy and Analysis*; CRC Press: Boca Raton, FL, USA, 2000.
27. Neagu, D.; Kyriakou, V.; Roiban, I.L.; Aouine, M.; Tang, C.Y.; Caravaca, A.; Kousi, K.; Schreur-Piet, I.; Metcalfe, I.S.; Vernoux, P.; et al. In Situ Observation of Nanoparticle Exsolution from Perovskite Oxides: From Atomic Scale Mechanistic Insight to Nanostructure Tailoring. *ACS Nano* **2019**, *13*, 12996–13005. [CrossRef]
28. Kim, Y.H.; Kang, Y.; Jo, S.; Jeong, H.; Neagu, D.; Myung, J.-H. Shape-shifting nanoparticles on a perovskite oxide for highly stable and active heterogeneous catalysis. *J. Chem. Eng.* **2022**, *441*, 136025. [CrossRef]
29. Schrenk, F.; Lindenthal, L.; Drexler, H.; Rameshan, R.; Summerer, H.; Berger, T.; Ruh, T.; Opitz, A.K.; Rameshan, C. Impact of nanoparticle exsolution on dry reforming of methane: Improving catalytic activity by reductive pre-treatment of perovskite-type catalysts. *Appl. Catal. B* **2022**, *318*, 121886. [CrossRef]
30. Han, J.W.; Park, J.S.; Choi, M.S.; Lee, H. Uncoupling the size and support effects of Ni catalysts for dry reforming of methane. *Appl. Catal. B* **2017**, *203*, 625–632. [CrossRef]
31. Gao, Y.; Chen, D.; Saccoccio, M.; Lu, Z.; Ciucci, F. From material design to mechanism study: Nanoscale Ni exsolution on a highly active A-site deficient anode material for solid oxide fuel cells. *Nano Energy* **2016**, *27*, 499–508. [CrossRef]
32. Merino, N.A.; Barbero, B.P.; Eloy, P.; Cadus, L.E. $La_{1-x}Ca_xCoO_3$ perovskite-type oxides: Identification of the surface oxygen species by XPS. *Appl. Surf. Sci.* **2006**, *253*, 1489–1493. [CrossRef]
33. Wang, Y.; Ren, W.; Liu, P.R.; Zhao, H.J.; Chen, J.; Deng, J.X.; Xing, X.R. Improved conductivity of $NdFeO_3$ through partial substitution of Nd by Ca: A theoretical study. *Phys. Chem. Chem. Phys.* **2015**, *17*, 29097–29102. [CrossRef]
34. Pishahang, M.; Mohn, C.E.; Stolen, S.; Bakken, E. DFT-study of the energetics of perovskite-type oxides $LaMO_3$ (M = Sc-Cu). *RSC Adv.* **2012**, *2*, 10667–10672. [CrossRef]
35. Torres, A.; Luque, F.J.; Tortajada, J.; Arroyo-de Dompablo, M.E. DFT investigation of Ca mobility in reduced-perovskite and oxidized-marokite oxides. *Energy Storage Mater.* **2019**, *21*, 354–360. [CrossRef]
36. Wexler, R.B.; Gautam, G.S.; Stechel, E.B.; Carter, E.A. Factors Governing Oxygen Vacancy Formation in Oxide Perovskites. *J. Am. Chem. Soc.* **2021**, *143*, 13212–13227. [CrossRef]
37. Cardona, J.F.Z.; Sacanell, J.; Barral, M.A.A.; Vildosola, V.; Viva, F. CO_2 reduction on a nanostructured $La_{0.5}Ba_{0.5}CoO_3$ perovskite: Electrochemical characterization and DFT calculations. *J. CO2 Util.* **2022**, *59*, 101973. [CrossRef]
38. Huang, R.; Lim, C.; Jang, M.G.; Hwang, J.Y.; Han, J.W. Exsolved metal-boosted active perovskite oxide catalyst for stable water gas shift reaction. *J. Catal.* **2021**, *400*, 148–159. [CrossRef]
39. Bare, Z.J.L.; Morelock, R.J.; Musgrave, C.B. Dataset of theoretical multinary perovskite oxides. *Sci. Data* **2023**, *10*, 244. [CrossRef] [PubMed]
40. Say, Z.; Dogac, M.; Vovk, E.I.; Kalay, Y.E.; Kim, C.H.; Li, W.; Ozensoy, E. Palladium doped perovskite-based NO oxidation catalysts: The role of Pd and B-sites for NO_x adsorption behavior via in-situ spectroscopy. *Appl. Catal. B* **2014**, *154*, 51–61. [CrossRef]
41. Maneerung, T.; Hidajat, K.; Kawi, S. K-doped $LaNiO_3$ perovskite for high-temperature water-gas shift of reformate gas: Role of potassium on suppressing methanation. *Int. J. Hydrogen Energy* **2017**, *42*, 9840–9857. [CrossRef]
42. Qi, R.; Jin, R.; An, L.; Bai, X.; Wang, Z.-J. A Ni/perovskite catalyst with low metal content for CO_2 reforming of methane. *Catal. Commun.* **2022**, *163*, 106419. [CrossRef]
43. Lai, K.Y.; Manthiram, A. Self-Regenerating Co-Fe Nanoparticles on Perovskite Oxides as a Hydrocarbon Fuel Oxidation Catalyst in Solid Oxide Fuel Cells. *Chem. Mater.* **2018**, *30*, 2515–2525. [CrossRef]
44. Lindenthal, L.; Popovic, J.; Rameshan, R.; Huber, J.; Schrenk, F.; Ruh, T.; Nenning, A.; Löffler, S.; Opitz, A.K.; Rameshan, C. Novel perovskite catalysts for CO_2 utilization—Exsolution enhanced reverse water-gas shift activity. *Appl. Catal. B* **2021**, *292*, 120183. [CrossRef]
45. Efimov, K.; Czuprat, O.; Feldhoff, A. In-situ X-ray diffraction study of carbonate formation and decomposition in perovskite-type BCFZ. *J. Solid State Chem.* **2011**, *184*, 1085–1089. [CrossRef]

46. Deka, D.J.; Kim, J.; Gunduz, S.; Aouine, M.; Millet, J.M.M.; Co, A.C.; Ozkan, U.S. Investigation of hetero-phases grown via in-situ exsolution on a Ni-doped (La,Sr)FeO_3 cathode and the resultant activity enhancement in CO_2 reduction. *Appl. Catal. B* **2021**, *286*, 119917. [CrossRef]
47. Zhang, T.; Zhao, Y.; Zhang, X.; Zhang, H.; Yu, N.; Liu, T.; Wang, Y. Thermal Stability of an in Situ Exsolved Nanoparticle Structured Perovskite Type Hydrogen Electrode for Solid Oxide Cells. *ACS Sustain. Chem. Eng.* **2019**, *7*, 17834–17844. [CrossRef]